Molecular Biology of the Cell
Vol. 12, 1995–2009, July 2001

Microtubule-dependent Changes in Assembly of Microtubule Motor Proteins and Mitotic Spindle Checkpoint Proteins at PtK1 Kinetochores

David B. Hoffman,* Chad G. Pearson,* Tim J. Yen,† Bonnie J. Howell,* and E.D. Salmon*‡

*Department of Biology, University of North Carolina, Chapel Hill, North Carolina 27599-3280; and †Fox Chase Cancer Center, Philadelphia, Pennsylvania

Submitted December 18, 2000; Revised April 9, 2001; Accepted April 27, 2001
Monitoring Editor: J. Richard McIntosh

The ability of kinetochores to recruit microtubules, generate force, and activate the mitotic spindle checkpoint may all depend on microtubule- and/or tension-dependent changes in kinetochore assembly. With the use of quantitative digital imaging and immunofluorescence microscopy of PtK1 tissue cells, we find that the outer domain of the kinetochore, but not the CREST-stained inner core, exhibits three microtubule-dependent assembly states, not directly dependent on tension. First, prometaphase kinetochores with few or no kinetochore microtubules have abundant punctate or oblate fluorescence morphology when stained for outer domain motor proteins CENP-E and cytoplasmic dynein and checkpoint proteins BubR1 and Mad2. Second, microtubule depolymerization induces expansion of the kinetochore outer domain into crescent and ring morphologies around the centromere. This expansion may enhance recruitment of kinetochore microtubules, and occurs with more than a 20- to 100-fold increase in dynein and relatively little change in CENP-E, BubR1, and Mad2 in comparison to prometaphase kinetochores. Crescents disappear and dynein decreases substantially upon microtubule reassembly. Third, when kinetochores acquire their full metaphase complement of kinetochore microtubules, levels of CENP-E, dynein, and BubR1 decrease by three- to sixfold in comparison to unattached prometaphase kinetochores, but remain detectable. In contrast, Mad2 decreases by 100-fold and becomes undetectable, consistent with Mad2 being a key factor for the "wait-anaphase" signal produced by unattached kinetochores. Like previously found for Mad2, the average amounts of CENP-E, dynein, or BubR1 at metaphase kinetochores did not change with the loss of tension induced by taxol stabilization of microtubules.

INTRODUCTION

Vertebrate kinetochores have three important functions in mitosis (reviewed in Rieder and Salmon, 1998; Skibbers and Hieter, 1998; Maney *et al.*, 2000; Shah and Cleveland, 2000). In prometaphase, they capture the growing plus ends of polar microtubules to form kinetochore microtubules that tether the kinetochore to the pole. This "search-and-capture" mechanism is facilitated by stochastic growth and shortening (dynamic instability) of polar spindle microtubules at their plus ends, multiple binding sites for plus ends at kinetochores, and microtubule motor proteins bound to kinetochores. These motors include cytoplasmic dynein and the kinesin-related protein CENP-E. A second function of kinetochores, and particularly their motor proteins, is to couple force production for chromosome movement at the kinetochore to assembly/disassembly of kinetochore microtubules at their plus end attachment sites. The third function of kinetochores is to prevent anaphase onset until all the chromosomes have become properly aligned on the spindle. Mitotic spindle checkpoint proteins at the kinetochore, Bub1, BubR1, Bub3, Mad1, and Mad2 sense the lack of tension and/or the lack of kinetochore microtubules at unattached kinetochores. This appears to block anaphase by promoting Mad2 binding and inhibition of Cdc20, the activator of the anaphase-promoting complex/cylosome.

Important for kinetochore function is the modification of kinetochore assembly produced by kinetochore and nonkinetochore spindle microtubules. There is qualitative evidence that unattached prometaphase kinetochores are larger in width (Rieder, 1982; Salmon, 1989; Cassimeris *et al.*, 1990) and have greater amounts of microtubule motor proteins and mitotic spindle checkpoint proteins (Gorbsky and Ricketts, 1993; Chen *et al.*, 1996; Echeverri *et al.*, 1996; Li and

‡ Corresponding author. E-mail address: tsalmon@email.unc.edu.

Benezra, 1996; Taylor and McKeon, 1997; Yao *et al.*, 1997, 2000; Chan *et al.*, 1998; Chen *et al.*, 1998; Dujardin *et al.*, 1998; Jablonksi *et al.*, 1998; Waters *et al.*, 1998; Martinez-Exposito *et al.*, 1999; King *et al.*, 2000) than metaphase kinetochores with their full complement of kinetochore microtubules. The enhanced assembly may be important for the recruiting kinetochore microtubules, increasing force production, and generating a strong "wait-anaphase" signal (Rieder and Salmon, 1998; Howell *et al.*, 2000). There is also evidence that kinetochore assembly depends on interactions with nonkinetochore microtubules. When all spindle microtubules are completely depolymerized, kinetochores, immunofluorescently stained for CENP-E, cytoplasmic dynein, and Bub3, are reported to expand from the small punctate or oblate fluorescence morphology typical of early prometaphase or metaphase kinetochores, into a "crescent" morphology extending around the centromere (Echeverri *et al.*, 1996; Thrower *et al.*, 1996; Martinez-Exposito *et al.*, 1999). This expanded crescent morphology may be a microtubule-dependent response of kinetochore assembly designed to substantially increase the solid angle for recruiting kinetochore microtubules under conditions where the density of spindle microtubules is very low. Conversely, kinetochores need to lose their expanded morphology upon kinetochore microtubule formation to prevent errors in chromosome segregation induced by attachment of individual kinetochores to microtubules from opposite poles (merotelic attachment; Cimini *et al.* 2001) in addition to turning off the wait-anaphase signal of the mitotic spindle checkpoint (Rieder and Salmon, 1998; Howell *et al.*, 2000).

To measure microtubule-dependent changes in kinetochore assembly, we have used digital imaging microscopy and quantitative immunofluorescence measurements of kinetochores in PtK1 cells under three microtubule states: unattached kinetochores in the absence of microtubules in cells treated with the microtubule-depolymerizing drug nocodazole; unattached or newly attached kinetochores (no or few kinetochore microtubules) in prometaphase cells with normal spindle assembly; and attached kinetochores on metaphase chromosomes with their full complement of kinetochore microtubules (~25 for PtK1 cells; McEwen *et al.*, 1997). We also tested whether loss of tension at metaphase kinetochores changes kinetochore assembly when kinetochore microtubules are preserved with the microtubule-stabilizing drug taxol (McEwen *et al.*, 1997; Waters *et al.*, 1998). Kinetochore tension generated by kinetochore pulling forces along kinetochore microtubules, like kinetochore microtubule formation, has been proposed to be an important regulator of mitotic spindle checkpoint activity (Nicklas *et al.* 1995; Nicklas, 1997; Waters *et al.*, 1999).

The proteins we analyzed were selected because of their location within the kinetochore and/or their potential function in recruitment of kinetochore microtubules, force generation, or the mitotic spindle checkpoint. Conventional electron microscopy has shown for vertebrate kinetochores a trilaminar plate structure. There is an inner core, containing a centromere-bound inner plate, and an outer domain, extending from the inner plate through a low-density gap to an outer plate, which contains attachment sites for the ends of kinetochore microtubules and an exterior fibrous corona (Rieder, 1982; Cassimeris *et al.*, 1990). We labeled the inner core of PtK1 kinetochores with human autoimmune CREST antibodies, which are polyspecific and bind to proteins CENP-A, CENP-B, and CENP-C (Earnshaw and Rothfield, 1985; Earnshaw *et al.*, 1989). CENP-A and CENP-C localize to the inner plate, whereas CENP-B is bound to nearby centromeric chromatin (Maney *et al.*, 2000). For outer domain components, we used antibodies to the microtubule motor proteins CENP-E and cytoplasmic dynein that have been localized to the outer plate and fibrous corona, consistent with their role in recruiting kinetochore microtubules and in force generation (reviewed in Rieder and Salmon, 1998; Maney *et al.*, 2000). We also used antibodies to the mitotic spindle checkpoint proteins, BubR1 (a kinase, related to budding yeast Mad3; Chan *et al.* 1998, 1999; Hardwick *et al.*, 2000) and Mad2 (Chen *et al.*, 1996; Li and Benezra, 1996). The only known mitotic spindle checkpoint protein that has thus far been localized ultrastructurally within the kinetochore is BubR1. It is found in the outer kinetochore domain, mainly at the outer plate with some at the inner plate (Jablonski *et al.*, 1998). Another factor related to the spindle checkpoint is the 3F3/2 antigen that has been detected by electron microscopy in the interzone between inner and outer plates (Campbell and Gorbsky, 1995). The 3F3/2 antibody recognizes a phosphorylated epitope at unattached kinetochores not under tension (Gorbsky and Ricketts, 1993; Campbell and Gorbsky, 1995; Nicklas *et al.*, 1995). By comparing the localization of Mad2 to BubR1, CENP-E, cytoplasmic dynein, 3F3/2 antigen, and CREST antigens at kinetochores in nocodazole-treated cells, we initially show that Mad2 is also localized to the outer kinetochore domain. We then examine the microtubule- or tension-dependent changes in assembly of CREST antigens, CENP-E, cytoplasmic dynein, BubR1, and Mad2 at kinetochores.

MATERIALS AND METHODS

Cell Culture and Drug Treatment

PtK1 cells (American Type Culture Collection, Rockville, MD) were maintained in Ham's F-12 (Sigma) containing 10% fetal bovine serum, penicillin, streptomycin, and amphotericin B (antimycotic) in a 37°C, 5% CO_2 incubator. For experiments in which cells were treated with nocodazole, a 10 mM stock in dimethyl sulfoxide (Sigma) was diluted into media for a final concentration of 20 μM. Standard media were replaced with media containing the nocodazole, and cells were returned to the 37°C incubator for the prescribed period of time before being removed for immunofluoresence labeling or for drug washout. Cells that were washed after a nocodazole treatment were first placed within two successive Petri dishes containing 3 ml of standard media, for 30 s each. Cells were then dipped four times in standard media at 37°C and placed within a second dish of standard media for 30 min before the coverslips were processed for immunofluorescence. To inhibit proteasome activity, MG-132 (Calbiochem, San Diego, CA) was added at 10 μM the culture media. For experiments in which cells were incubated with taxol (Sigma), a 10 mM stock in dimethyl sulfoxide was diluted into standard media for a final concentration of 10 μM. Standard media were then replaced with media containing the taxol, and cells were returned to the 37°C incubator for 45 min before removal for immunofluorescence processing. In cases where it was desired to test for the possible steric hindrance effect of microtubules (i.e., blocking of antibody staining) at the kinetochore, cells were first lysed with 0.5% Triton X-100 in PHEM buffer [60 mM piperazine-*N*,*N*′-bis(2-

ethanesulfonic acid), 25 mM HEPES, 10 mM EGTA, 4 mM $MgSO_4$ at pH 7.0] in the presence of 4 mM MgATP for 5 min at room temperature. After four, 5-min rinse periods in PHEM, cells were incubated for 2 h at 4°C in a high Ca^{2+} buffer [60 mM piperazine-*N*,*N*′-bis(2-ethanesulfonic acid), 25 mM HEPES, 4 mM $MgCl_2$, and 10 mM $CaCl_2$ at pH 7.0]. Fixation and immunofluorescence labeling procedures followed.

Immunofluorescence

Immunofluorescence labeling procedures were conducted at room temperature. Cells were first lysed in freshly prepared 0.5% Triton X-100 in PHEM buffer for 5 min. When staining for the phosphoprotein recognized by the 3F3/2 antibody, 100 nM microcystin (Sigma) was included in the lysis buffer (Waters *et al.*, 1998). Cells were then fixed in 4% formaldehyde (prepared fresh daily from paraformaldehyde) for 20 min. Next, cells were rinsed in phosphate-buffered saline/Tween (PBST) (PBS: 140 mM NaCl, 2.5 mM KCl, 1.6 mM KH_2PO_4, 15 mM Na_2HPO_4, pH 7.2, with 0.05% Tween 20) and subsequently blocked in 5% boiled donkey serum in PHEM for at least 45 min. Incubation in primary antibodies (diluted into 5% donkey serum in PHEM) followed for 45 min, after which time cells were rinsed four times in PBST and then incubated for 45 min in secondary donkey anti-rabbit, anti-mouse, or anti-human antibodies (diluted 1:100 in 5% donkey serum in PHEM), conjugated to Rhodamine Red-X (Jackson ImmunoResearch; West Grove, PA). For costaining experiments with two kinetochore proteins, cells were incubated simultaneously with antibodies to both proteins as described above for single antibodies. After PBST rinses, cells were incubated with appropriate secondary antibodies. Fluorescein-conjugated donkey anti-mouse secondary antibodies specific to anti-dynein primaries were incubated concurrently with Rhodamine Red-X-conjugated donkey anti-rabbit antibodies when labeling for dynein together with BubR1, CENP-E, or Mad2 proteins. For simultaneous Mad2 and CREST labeling, Rhodamine Red-X donkey anti-rabbit (specific to anti-Mad2 primaries) and Alexa Fluor 488-conjugated goat anti-human secondary antibodies (Molecular Probes, Eugene, OR) were incubated together.

CREST serum was a gift from Dr. B.R. Brinkley (Baylor College of Medicine, Houston, TX) and used at 1:750 dilution. Affinity-purified CENP-E and BubR1 antibodies (Chan *et al.*, 1998, 1999) were used at 1:500 dilution. The monoclonal antibody to the 3F3/2 phosphoepitope (provided by Dr. Gary Gorbsky, University of Oklahoma Health Sciences Center, Oklahoma City, OK) was used at 1:1500 dilution. Antibodies to Mad2 were affinity-purified as described in Waters *et al.* (1998) and used at 1:100 dilution. The monoclonal antibody to the 70.1 IC of cytoplasmic dynein (Sigma D5167) was used at 1:2000 dilution. Immunostained cells were mounted onto precleaned microscopy slides in 90% glycerol, 10% Tris buffer with 0.5–1% n-propyl galate for subsequent viewing.

Microscopy and Image Acquisition

Immunofluorescently labeled cells were viewed with a multimode digital fluorescence microscope system (Salmon *et al.*, 1994). Images were obtained with a Hamamatsu C4880 cooled charge-coupled device digital camera (12-μm square pixels), with the use of a Nikon Microphot FX-A microscope equipped with a 60X/1.4 NA objective lens and a 2.0x optivar projection lens. Both differential interference contrast (DIC) and fluorescence images were obtained for control metaphase cells and for experimental cells. To determine the progress of a control cell through the stages proceeding nuclear envelope breakdown, phase contrast microscopy was used to view the maturation stage of chromosomes within the nucleus with the use of a 60X/1.4 NA phase 3 objective lens. Digital images were acquired by MetaMorph image processing software (Universal Imaging, West Chester, PA). Z-series optical sections through each cell analyzed were obtained at 0.5-μm steps, with the use of MetaMorph software and a Ludl (Hawthorne, NY) stepping motor.

Data Analysis and Presentation

We used a method described by King *et al.* (2000) for measuring kinetochore fluorescence with the use of MetaMorph imaging software and the primary 12-bit image stacks. Images were not deconvolved and the focal depth of the NA = 1.4 objective was usually sufficient to include the great majority of the fluorescence from the full depth of a kinetochore (King *et al.*, 2000). Typically, the central fluorescence of a kinetochore was dim 0.5 μm from best focus and not apparent by 1 μm. Adjacent kinetochores in the *z*-axis direction were rarely within 1 μm of each other in PtK1 cells. For fluorescence measurements, the best in-focus image of a kinetochore was determined visually by stepping through the *z*-axis stacks of corresponding DIC and fluorescence images (see RESULTS). Computer-generated 9 × 9 and 13 × 13 pixel regions were centered over each kinetochore (Figure 3) and the total integrated fluorescence counts were obtained for each region. The 9 × 9 pixel region corresponded to a 0.9 × 0.9 μm region that was typically large enough to contain 90% of kinetochore fluorescence, except for the highly expanded kinetochores in nocodazole-treated cells. The outer region, 1.3 × 1.3 μm, was chosen to be more than twice the area of the inner region, but not so large as to include significant fluorescence from a sister kinetochore; the center-to-center distance between sister kinetochores in nocodazole-treated cells or prophase cells, is only 0.9–1.1 μm. Inner and outer region data were transferred into Microsoft Excel (Microsoft, Richmond, WA) with the use of the MetaMorph Dynamic Data Exchange function. The measured value for the 9 × 9 pixel region includes both kinetochore fluorescence and local background fluorescence. The background component was obtained by subtracting the integrated value of the 9 × 9 pixel region from the larger 13 × 13 pixel region. This result was scaled in proportion to the smaller area of the 9 × 9 pixel region and then subtracted from the integrated value of the 9 × 9 pixel region to yield a value for kinetochore fluorescence (minus background, see equation in Figure 3). As pointed out by King *et al.* (2000), this method has major advantages over the use of an arbitrary spindle region for measuring background fluorescence because it controls for inhomogeneity in background fluorescence. Increasing the inner and outer measurement regions to 10 × 10 and 14 × 14 pixels, respectively, increased measured values of kinetochore fluorescence by ~10% when sister kinetochores were well separated, but caused problems when they were close together. Average values of kinetochore fluorescence were calculated from no fewer than 50 kinetochores for each experimental condition. Two-tailed *t* statistical tests were performed among treatment types for each kinetochore protein.

The center-to-center distances between sister kinetochores were measured in prophase cells, in control metaphase cells and in cells that were treated with taxol or nocodazole, as described above. Primary 12-bit image stacks were calibrated at the appropriate pixel-to-micrometer ratio with the use of the MetaMorph imaging software, and interkinetochore distances were measured with the use of linear pixel regions. To measure the distances between sister kinetochores, which appeared at their brightest on different image planes (indicating a positional separation along the *z*-axis), measured *x*- and *y*-axis distances were triangulated and solved for the resulting distance vector. Data were recorded onto Microsoft Excel spreadsheets.

Presentation images were created by first converting the 12-bit digital images to 8-bit with the use of MetaMorph software and importing the images into Adobe Photoshop 5.0 (Adobe, Mountain View, CA), where they were sized, contrast-enhanced, pseudocolored, and/or overlaid. Final images were montaged and labeled with the use of CorelDRAW 7 (Corel, Ottawa, Canada).

RESULTS

Mad2, Like CENP-E, Cytoplasmic Dynein, BubR1, Bub3, and 3F3/2, Localizes to Kinetochore Outer Domain Crescents in the Absence of Spindle Microtubules

To determine whether Mad2 binds to the kinetochore outer domain, we took advantage of the morphological changes that occur for unattached kinetochores when depleted of spindle microtubules for several hours by inhibition of microtubule assembly with nocodazole (DeBrabender *et al.*, 1981; Thrower *et al.*, 1996). We found that a 4-h treatment of PtK1 cells in 20 μM nocodazole caused Mad2 along with CENP-E, cytoplasmic dynein, and Bub1R, but not the inner core CREST antigens, to assemble into an expanded crescent, or C-shape (Figure 1). These crescents were often observed to form a ring around the centromere region (Figure 1). Figure 1D shows an example of the outer domain labeled with Mad2 antibody extending beyond the punctate inner core labeled with CREST antibody. The crescent reconfiguration of kinetochore outer domain morphology indicates that Mad2, like cytoplasmic dynein, CENP-E, BubR1, Bub3 (Martinez-Exposito *et al.*, 1999), and 3F3/2 antigen (Cimini *et al.*, 2000) assembles onto sites within the outer domain.

The formation of outer domain crescents and rings was only observed in cells that had undergone complete microtubule disassembly by prolonged incubations (30 min to 4 h) in 20 μM nocodazole. None of the 50 or more unattached or newly attached kinetochores measured in control prometaphase cells showed crescent or ring morphologies.

Incubation of cells in nocodazole prolongs the duration of mitosis by spindle checkpoint activation. This raises the possibility that the expanded crescent morphologies of kinetochores seen after 4 h in nocodazole are a product of the duration of mitosis independent of microtubule disassembly. To test this possibility, we arrested cells in metaphase with the use of 10 μM MG-132 to block the proteasome activity needed for anaphase onset (Clute and Pines, 1999; Josefseberg *et al.*, 2000). After 4 h in the inhibitor, chromosomes exhibited normal metaphase behaviors, oscillating back and forth along the spindle axis near the spindle equator (Khodjakov and Rieder, 1996). Kinetochores in cells fixed and stained with CENP-E antibodies did not show the expanded crescent morphology typical of kinetochores in cells depleted of microtubules for 4 h by nocodazole (Figure 1B), but the more punctuate staining typical of normal metaphase kinetochores (see Figure 6 for typical metaphase staining). The distance between sister kinetochores was 2.6 $\pm$ 0.4 μm (n = 46), very similar to the 2.5 $\pm$ 0.4 μm (n = 47) measured for stretched centromeres in control cells. These results indicate that the remodeling of the kinetochore that occurs with nocodazole treatment is not simply a consequence of the duration of mitosis.

Kinetochores in Prophase Nuclei Lack Cytoplasmic Dynein, BubR1, and Crescent Morphology

We found that kinetochores at late prophase in PtK1 cells stained brightly for CENP-E, Mad2, and the 3F3/2 antigen, but not for cytoplasmic dynein or BubR1 (Figure 2). Cytoplasmic dynein and Bub1R bind kinetochores after nuclear envelope breakdown and entry into prometaphase (Figure

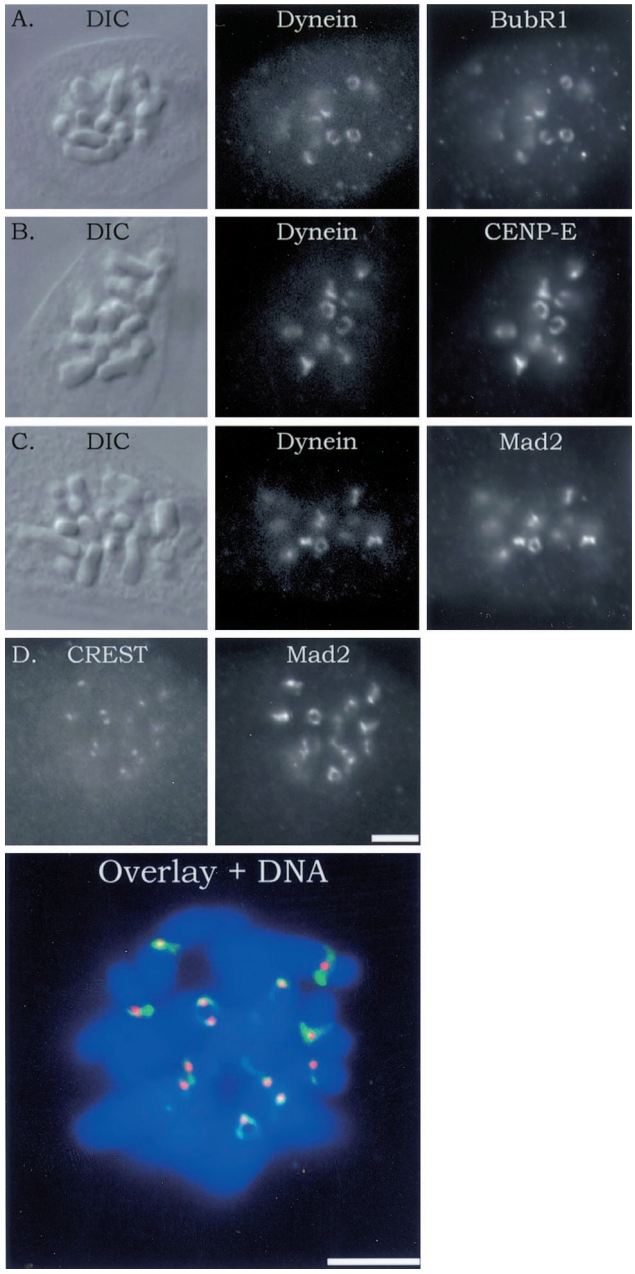

Figure 1. Immunofluorescence colocalization of BubR1, CENP-E, and Mad2 with cytoplasmic dynein to the kinetochore outer domain. Kinetochore outer domain crescents were induced by incubation of mitotic cells for 4 h in 20 μM nocodazole to completely depolymerize spindle and kinetochore microtubules. Rows contain images of the same cell. (A–C) Left column shows DIC images of the cells, the center column shows fluorescein isothiocyanate fluorescence of cytoplasmic dynein, and the right column shows rhodamine fluorescence staining of BubR1, CENP-E, or Mad2. (D) Left frame is CREST staining, the right is Mad2 staining, and the lower is a color overlay for the same cell, with 4,6-diaminidino-2-phenylindole (DAPI) staining for DNA. Note again that Mad2, like BubR1, CENP-E, and cytoplasmic dynein, localizes to the outer domain crescents. CREST staining is restricted to the kinetochore inner core. Scale, 10 μm.

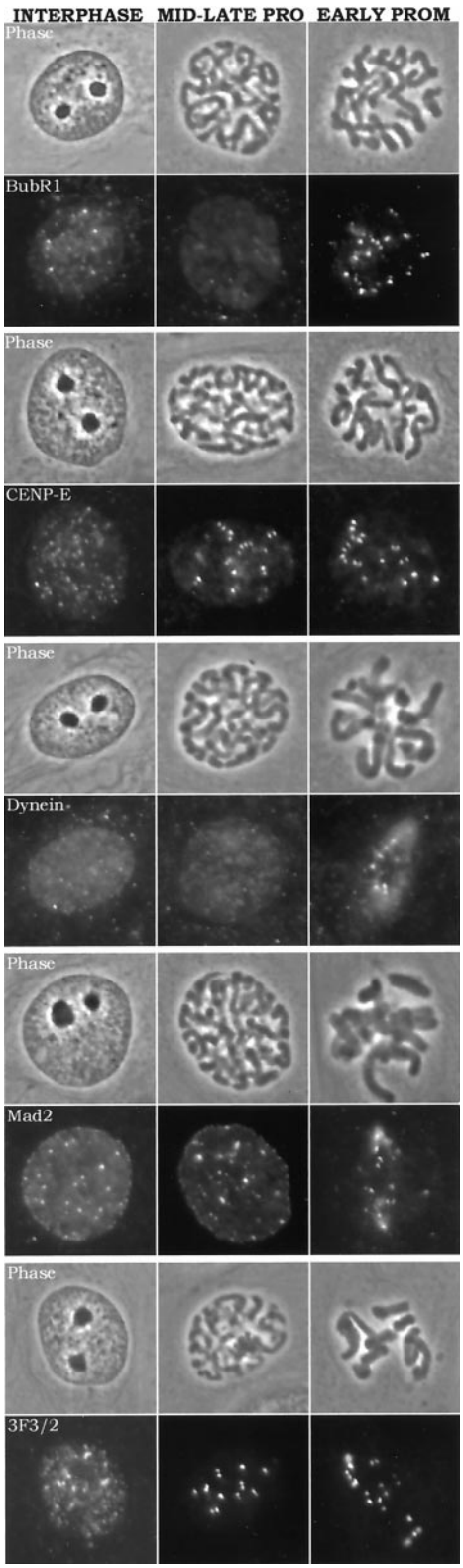

Figure 2. Immunofluorescence staining for BubR1, CENP-E, cytoplasmic dynein, Mad2, and the 3F3/2 antigen in control interphase, mid-to-late prophase, and early prometaphase cells. Phase contrast and rhodamine fluorescence images are shown for interphase cells (left), mid-to-late-prophase cells (center), and early prometaphase cells (right). Only CENP-E, Mad2, and 3F3/2 antigens appear at kinetochores during prophase, whereas BubR1 and cytoplasmic dynein do not become evident at kinetochores until after nuclear envelope breakdown. No crescent or ring morphologies were seen for prometaphase kinetochores. Scale: 10 μm = 0.33 in.

2). Because prophase nuclei are devoid of microtubules like mitotic cells treated with nocodazole, we asked whether kinetochores in prophase nuclei also exhibit crescent or ring morphologies. However, no kinetochore crescent or ring morphologies were seen for the proteins examined (Figure 2) in control or cells treated for 4 h in nocodazole, indicating that crescent formation is a property of prometaphase kinetochores.

Changes in Kinetochore Assembly Between Unattached Prometaphase Kinetochores and Metaphase Kinetochores

We used quantitative immunofluorescence microscopy to compare changes in different proteins at kinetochores relative to their values at fully attached and tense kinetochores on chromosomes aligned at the metaphase plate. For each cell analyzed, optical z-series of DIC and corresponding fluorescence images were obtained at 0.5-μm steps through the cell so that all sister kinetochore pairs in each PtK1 cell were available for quantitative fluorescence analysis. When the fluorescence of immunolabeled kinetochores was dim and therefore difficult to detect, the location of kinetochores was identified as increased "bumps" in the corresponding DIC images at the periphery of the centromeric constriction of the chromosome arms. Seven to 10 cells were analyzed for each protein and treatment. The integrated fluorescence of each immunostained antigen at a kinetochore was determined by quantitative image analysis as initially developed by King *et al.* (2000) and described in MATERIALS AND METHODS and Figure 3.

We first examined unattached kinetochores on mono-oriented chromosomes or leading kinetochores on congressing chromosomes (see diagram in Figure 4A) because these kinetochores have zero or one to three kinetochore microtubules, respectively, and can be considered together as unattached kinetochores (McEwen *et al.*, 1997). Figure 4B shows the differences in kinetochore fluorescence intensity between unattached kinetochores and kinetochores on metaphase-aligned chromosomes, which have a full complement of kinetochore microtubules. There are several important results. We saw no change in the inner core CREST fluorescence between unattached, leading, or metaphase kinetochores (Figure 4B). In contrast, all outer domain proteins decreased in integrated intensity at metaphase kinetochores (Figure 5 and Table 1), indicating that outer domain protein assembly is sensitive to kinetochore microtubule formation. The integrated intensity of CENP-E and BubR1 decreased at kinetochores by three- to fourfold upon metaphase alignment (Figure 5A), however, these proteins were still abundant and clearly visible on metaphase kinetochores (Figure 4B). Cytoplasmic dynein did not appear as concentrated on unattached or leading prometaphase kinetochores as

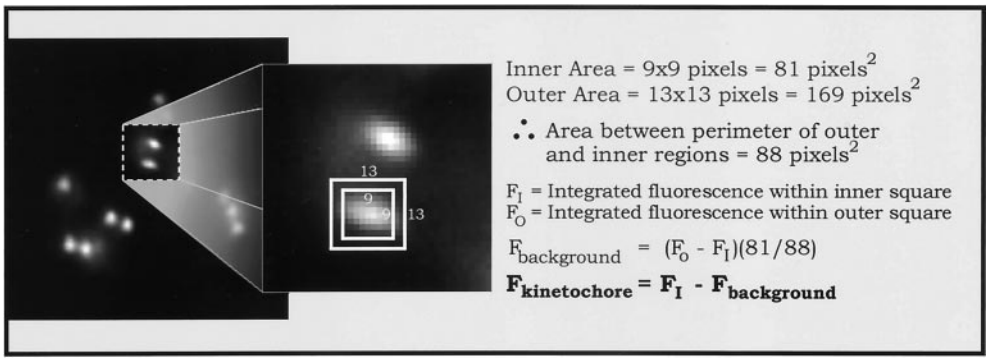

Figure 3. Analysis used to determine the integrated intensity of a given immunofluorescently stained kinetochore as diagrammed in the figure and described in MATERIALS AND METHODS. The great majority of kinetochore fluorescence is contained within the central 9 × 9 pixel square, which corresponds to a 0.9- × 0.9-μm square region of the specimen.

CENP-E and BubR1. The five- to sixfold decrease in cytoplasmic dynein fluorescence intensity upon metaphase alignment (Figure 5B) made fluorescence at the kinetochore barely visible, unlike the metaphase fluorescence of CENP-E and BubR1 (Figure 4B). Nevertheless, this weak fluorescence indicates that some cytoplasmic dynein remains on metaphase kinetochores. In contrast, Mad2 was not visible by eye above background fluorescence on metaphase kinetochores

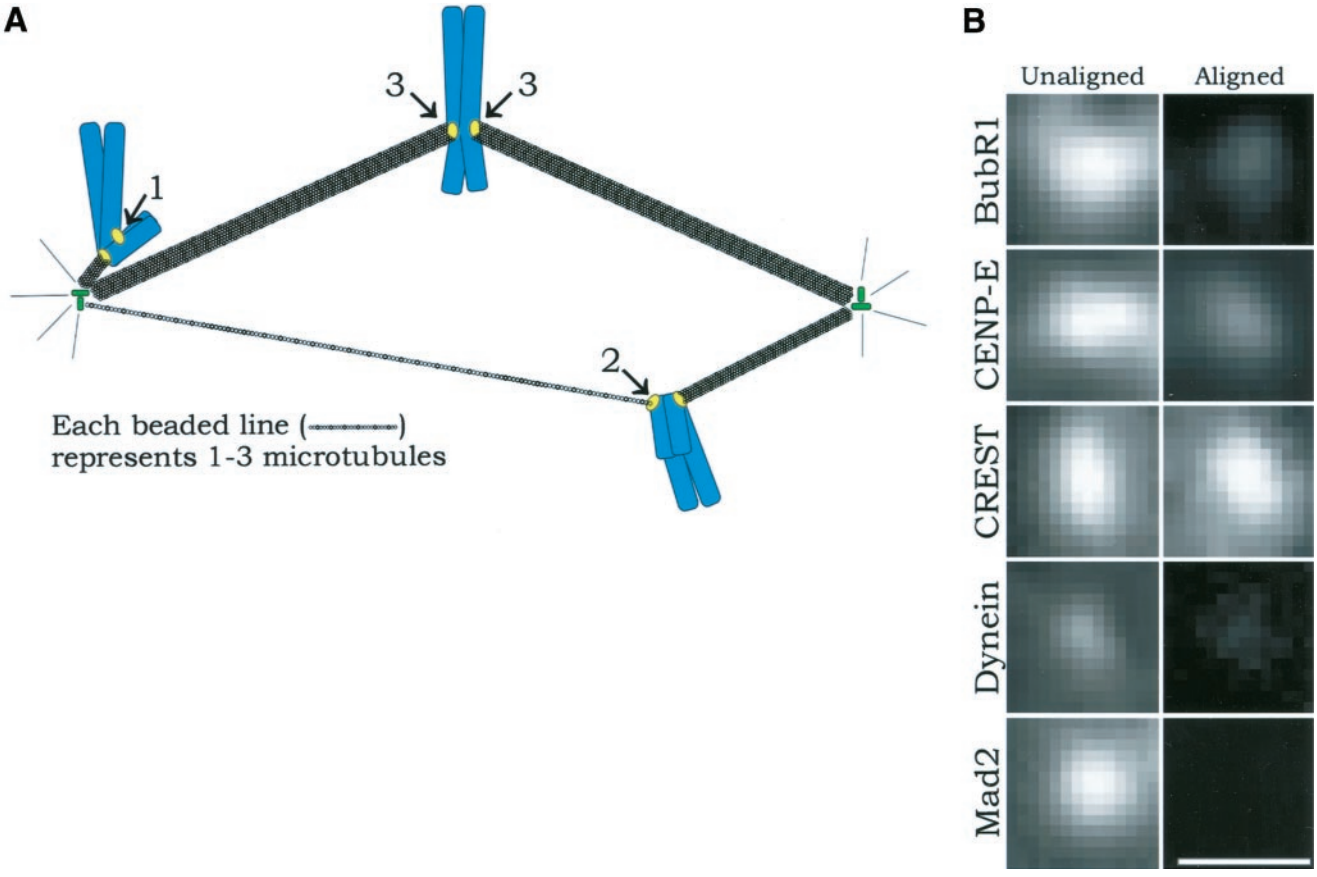

Figure 4. (A) Diagram showing relative numbers of kinetochore microtubules for unattached kinetochores on mono-oriented chromosomes (1; no kinetochore microtubules), leading kinetochores on congressing chromosomes (2; according to McEwen *et al*., 1997, these generally possess a few microtubules and can be grouped with unattached kinetochores), and fully attached kinetochores on chromosomes aligned at the metaphase plate (3; these are bound to mature kinetochore fibers, which contain ~25 microtubules [McEwen *et al*., 1997]) in prometaphase cells. Nonkinetochore spindle microtubules are not shown for clarity. (B) Immunofluorescence images comparing the fluorescence intensity of unattached or leading kinetochores of unaligned chromosomes and fully attached kinetochores of metaphase-aligned chromosomes for the proteins Bub1R, CENP-E, CREST, cytoplasmic dynein, and Mad2. CREST remains unchanged, BubR1 and CENP-E deplete to moderate levels, cytoplasmic dynein depletes to a low level, and Mad2 becomes undetectable. The pixel density in the photographic images is higher than in the original micrographs. Scale = 1 μm.

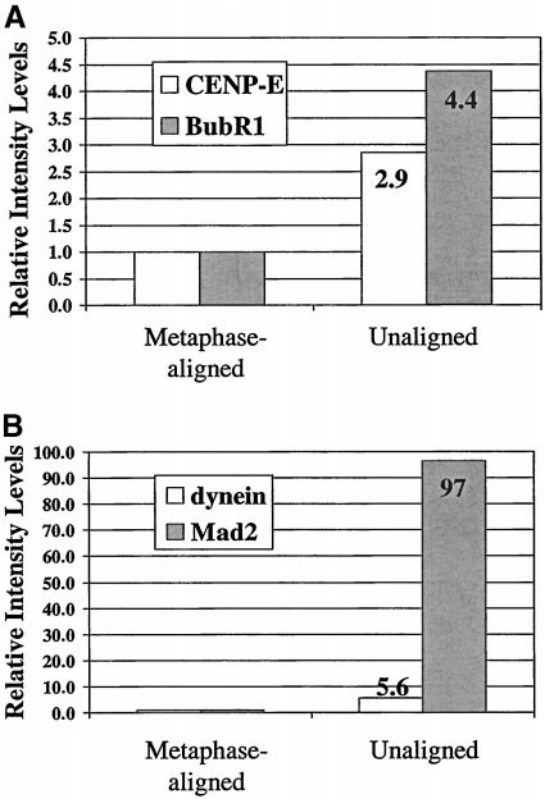

Figure 5. Quantitative comparisons of the relative changes in fluorescence of unattached or leading kinetochores in prometaphase (Figure 4A) labeled with CENP-E, and BubR1 antibodies in (A) and cytoplasmic dynein and Mad2 antibodies in (B) relative to kinetochores on chromosomes at the metaphase plate. Average values taken from Table 1 are normalized to those values for metaphase control cells. Note that unattached or leading kinetochores exhibit integrated fluorescence intensity levels relative to kinetochores of metaphase-aligned chromosomes of 4.4 for BubR1 (A), 2.9 for CENP-E (A), 5.6 for cytoplasmic dynein (B), and 97 for Mad2 (B).

(Figure 4B), but measurements indicated slightly higher levels than background (Table 1). In addition, Mad2 was measured to be 100-fold more abundant on unattached or leading kinetochores in prometaphase in comparison to kinetochores at metaphase (Figure 5B and Table 2). Thus, of all the proteins tested at kinetochores, Mad2 was the most sensitive to depletion by the microtubule attachment and/or tension achieved by metaphase kinetochores.

Prolonged Nocodazole Treatment Enhances Outer Domain Protein Assembly with a Dramatic Increase in Cytoplasmic Dynein

We asked how much the assembly of the inner core and kinetochore outer domain proteins change when kinetochores are deprived of interactions with microtubules for prolonged periods in the cells treated with 20 μM nocodazole for either 30 min or 4 h, to depolymerize all microtubules (Figure 6A). Previous studies have shown that in 20 μM nocodazole, nonkinetochore microtubules in prometaphase and metaphase cells disappear within 1–2 min, and kinetochore microtubules are not detectable in cells fixed for electron microscopy after 20 min (Cassimeris *et al.*, 1990). We found no changes in the amount of inner core CREST antigens at kinetochores in the nocodazole-treated cells. However, we did observe changes in the amounts of the outer domain proteins tested (Figures 6A and 7 and Table 2). Relative to metaphase kinetochores, the integrated fluorescence measured by our 0.9- $\times$ 0.9-μm measurement region centered on the kinetochore for CENP-E increased 2.5-fold at 30 min and by 3.8-fold at 4 h, whereas BubR1 increased by about the same amount, fourfold, at either 30 min or 4 h (Figures 6A and 7A). In contrast, the integrated fluorescence for cytoplasmic dynein and Mad2 measured in the same way both increased by 60-fold at 30 min and 100-fold at 4 h in the microtubule-depleted cells relative to untreated metaphase kinetochore values (Figures 6A and 7B). These measurements for CENP-E, BubR1, and Mad2 obtained for nocodazole-treated kinetochores are similar to the values we measured for unattached kinetochores in prometaphase. Surprisingly, the 60- and 100-fold values measured for cytoplasmic dynein at 30 min and 4 h, respectively, are much larger than predicted from the 5.5-fold value measured for unattached or leading kinetochores in prometaphase.

The above-mentioned integrated fluorescence measurements for kinetochore proteins in the nocodazole-treated cells may underestimate the actual values due to the expansion of the kinetochores into the crescent and ring morphologies beyond our 0.9- $\times$ 0.9-μm measurement region (Figure 3), particularly after 4 h in nocodazole (Figure 6A), and our inability to accurately measure contributions from the periphery of the crescents and/or rings. The errors in our average measurements are not likely to underestimate the actual values by more than a factor of 2 because crescent intensity decreased away from the center of the kinetochore and many kinetochores did not show rings.

With the release of tension that resulted from the nocodazole-induced disappearance of kinetochore microtubules, distances between sister kinetochores in cells treated with that drug for 30 min and 4 h decreased to 1.23 $\pm$ 0.13 μm (n =

Table 1. Integrated fluorescence for aligned versus unaligned kinetochores

	Aligned	Unaligned
BubR1		
n	26	13
mean $\pm$ SD	5311 $\pm$ 1870	23247 $\pm$ 6084
ratio to control	1	4.4
CENP-E		
n	51	22
mean $\pm$ SD	20469 $\pm$ 6773	58349 $\pm$ 16655
ratio to control	1	2.9
Dynein		
n	27	22
mean $\pm$ SD	355 $\pm$ 850	1986 $\pm$ 938
ratio to control	1	5.6
Mad2		
n	107	25
mean $\pm$ SD	95 $\pm$ 315	9178 $\pm$ 4173
ratio to control	1	97

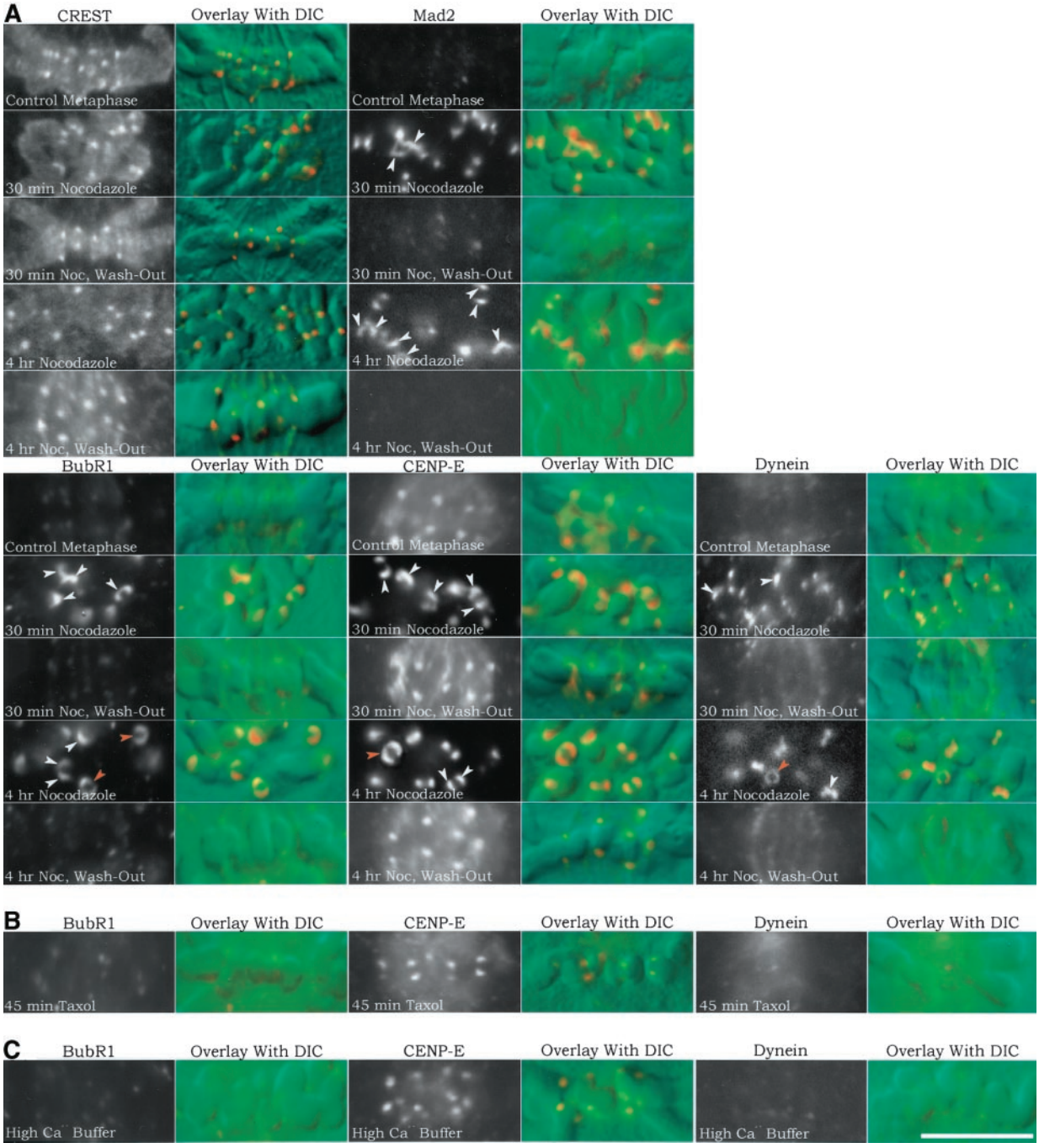

Figure 6. Kinetochore immunofluorescence and corresponding chromosome DIC image overlays of PtK1 cells treated with nocodazole, taxol, or high Ca^{2+} buffer. Changes in kinetochore protein localization were compared between control metaphase cells and cells treated with 20 μM nocodazole for 30 min or 4 h to induce prolonged microtubule disassembly or the same treatments followed by nocodazole washout for 30 min to induce microtubule reassembly and kinetochore microtubule formation (A); 10 μM taxol for 45 min to induce loss of kinetochore tension without major changes in kinetochore microtubule number (B); and high Ca^{2+} buffer at 4°C after cell lysis to induce disassembly of kinetochore microtubules and test for microtubule steric hindrance of antibody labeling (C). For each protein tested, both immunofluorescence and DIC images were recorded. The left column contains black-and-white rhodamine-fluorescence images of immunofluorescence all printed at the same contrast to show relative differences in immunostaining brightness levels. The right column contains color overlays of rhodamine fluorescence on the corresponding DIC images of the chromosomes. Color images were artificially contrast-enhanced to show location of kinetochores on the chromosomes. Arrowheads in the Mad2, BubR1, CENP-E, and cytoplasmic dynein images of cells treated with nocodazole for 30 min or 4 h indicate kinetochore crescent (white arrowheads) or ring-shaped (orange arrowheads) morphologies. Under all conditions tested, kinetochores stained with CREST maintained the same punctuate or oblate morphology. Scale, 10 μm.

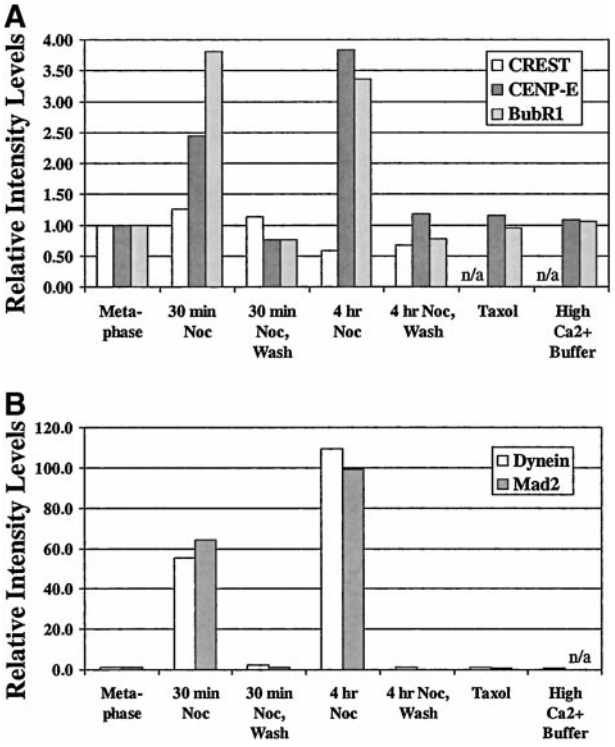

Figure 7. Quantitative comparisons of relative changes in fluorescence staining intensity of kinetochores labeled with CREST, CENP-E, and BubR1 antibodies in (A) and cytoplasmic dynein and Mad2 antibodies in (B) relative to kinetochores on metaphase chromosomes in control cells for the various experimental protocols listed along the *x*-axis. Average values taken from Table 2 are normalized to those values for metaphase control cells. Values underestimate total crescent fluorescence as described in RESULTS. Note in (A) that both CENP-E and BubR1 fluorescence at kinetochores in cells fixed after 30-min or 4-h nocodazole incubations showed increase in intensity in the range of 2.5- to 4-fold beyond control metaphase kinetochores. When subjected to taxol treatment to test for tension effects, or incubation in high Ca^{2+} buffer to test for microtubule steric hindrance, both CENP-E and BubR1 fluorescence at kinetochores was not changed from values for control metaphase cells. Note in (B) that both cytoplasmic dynein and Mad2 fluorescence at kinetochores in cells fixed after 30-min nocodazole incubations showed increase in intensity in the range of 55- to 65-fold increase beyond the control. After 4-h nocodazole incubation, both intensities increased further to 100- to 110-fold. Like CENP-E and BubR1, cytoplasmic dynein-stained kinetochores in metaphase cells that underwent taxol treatment or incubation in high Ca^{2+} buffer after cell lysis showed fluorescence that was similar to control metaphase kinetochores.

30) and 1.12 ± 0.16 μm (n = 34), respectively, from the observed control metaphase value of 2.43 ± 0.38 μm (n = 39). The values for interkinetochore distance in nocodazole-treated cells is similar to the distance recorded for sister kinetochores within prophase nuclei, 0.90 ± 0.13 μm (n = 48).

These changes in outer domain protein assembly and kinetochore morphology were reversible upon washing out nocodazole to induce spindle reassembly. By 30 min after washing out nocodazole, cells progressed to near metaphase and kinetochores exhibited the punctate morphology and integrated fluorescence intensity values of metaphase-aligned chromosomes in control cells (Figures 6A and 7 and Table 2). This demonstrates that the changes measured in kinetochore outer domain protein assembly and morphology depend directly on the absence or presence of microtubules.

Loss of Tension at Metaphase Kinetochores with Taxol-stabilized Microtubules Has Little Effect on Outer Domain Protein Assembly

Unattached kinetochores differ from kinetochores of chromosomes at the metaphase plate in two ways: they lack kinetochore microtubules and they are not under the tension produced by net pulling forces at attached kinetochores (Waters *et al.*, 1996b; Khodjakov and Rieder, 1996; Nicklas, 1997). Previously, Waters *et al.* (1998) tested for the contributions of tension in inducing the depletion of Mad2 at metaphase PtK1 kinetochores by treating metaphase cells for 45 min in 10 μM taxol, a microtubule-stabilizing drug (Waters *et al.*, 1996a). This treatment maintains the normal metaphase complement of kinetochores microtubules (McEwen *et al.*, 1997) while inducing the loss of kinetochore tension as measured by the lack of stretch of the interkinetochore centromere region (Waters *et al.*, 1996a). Waters *et al.* (1998) found that only a few kinetochores exhibited a detectable amount of Mad2 localization under these conditions. Subsequently, Martinez-Exposito *et al.* (1999) found no significant increase in Bub3 levels between untreated and taxol-treated metaphase kinetochores. In our tests for the effects of tension, we also found that the integrated fluorescence intensities of BubR1, CENP-E, cytoplasmic dynein, and Mad2 did not change their values at metaphase kinetochores after taxol treatment (Figure 6B and 7 and Table 2). Loss of tension at the kinetochores of taxol-treated cells was confirmed by the observation that the distance between sister kinetochores fell to ~1.20 ± 0.17 μm (n = 30), from the average metaphase control value of 2.43 ± 0.38 μm (n = 39).

Kinetochore Microtubules Do Not Sterically Hinder Antibody Binding in Our Immunofluorescence Assays

A possible error in with the use of immunofluorescence to measure the amount of protein at metaphase kinetochores is steric hindrance of antibody binding produced by the presence of kinetochore microtubules. This could reduce values measured for metaphase kinetochores with a full complement of kinetochore microtubules in comparison to unattached or leading kinetochores having no or very few kinetochore microtubules. A previous study by Waters *et al.* (1998) has shown that this steric hindrance is not a factor for immunofluorescence localization of Mad2 at kinetochores. Cells were treated with cold and high calcium concentrations after cell lysis to induce the disappearance of kinetochore microtubules before fixation for immunofluorescence. These cells exhibited no detectable Mad2 fluorescence on metaphase kinetochores and high levels of fluorescence on unattached or leading kineto-

Table 2. Integrated kinetochore fluorescence for various experimental protocols

A	Control	30-min Noc	30-min Noc, washout	4-h Noc	4-h Noc, washout
CREST					
n	63	56	63	60	63
mean ± SD	2753 ± 837	3463 ± 1005	3132 ± 886	1612 ± 404	1851 ± 514
ratio to control	1	1.3	1.1	0.6	0.7
BubR1					
n	51	53	51	52	50
mean ± SD	8792 ± 3161	33456 ± 7530	6794 ± 2846	29500 ± 6548	6834 ± 2948
ratio to control	1	3.8	0.8	3.4	0.8
CENP-E					
n	65	57	60	53	63
mean ± SD	23250 ± 6685	57026 ± 15865	17807 ± 5275	89049 ± 17746	27563 ± 6886
ratio to control	1	2.5	0.8	3.8	1.2
Dynein					
n	54	53	50	53	53
mean ± SD	120 ± 416	6629 ± 3238	286 ± 464	13182 ± 5713	120 ± 254
ratio to control	1	55	2.4	110	1.0
Mad2					
n	53	56	52	66	52
mean ± SD	125 ± 235	8030 ± 1978	138 ± 404	12365 ± 1641	3 ± 175
ratio to control	1	65	1.1	99	0.03

B	Control	45 min Taxol
BubR1		
n	56	51
mean ± SD	16624 ± 4679	15932 ± 5344
ratio to control	1	1.0
CENP-E		
n	56	57
mean ± SD	23346 ± 6153	26972 ± 8371
ratio to control	1	1.2
Dynein		
n	55	57
mean ± SD	1624 ± 511	1537 ± 575
ratio to control	1	1.0
Mad2		
n	75	67
mean ± SD	1557 ± 7818	1003 ± 3191
ratio to control	1	0.6

C	Control	High Ca^{2+} Buffer
BubR1		
n	61	51
mean ± SD	6568 ± 1769	6943 ± 2095
ratio to control	1	1.1
CENP-E		
n	57	53
mean ± SD	10216 ± 2759	11034 ± 3188
ratio to control	1	1.1
Dynein		
n	53	51
mean ± SD	1187 ± 346	906 ± 309
ratio to control	1	0.8

chores as measured for cells without extraction of kinetochore microtubules (Waters *et al*., 1998). We used similar procedures to test for steric hindrance by kinetochore microtubules at metaphase-aligned chromosomes for immunofluorescence analysis of BubR1, CENP-E, and cytoplasmic dynein. We found, as for Mad2, no evidence for steric hindrance by metaphase kinetochore microtubules in our analysis (Figure 6C and 7 and Table 2).

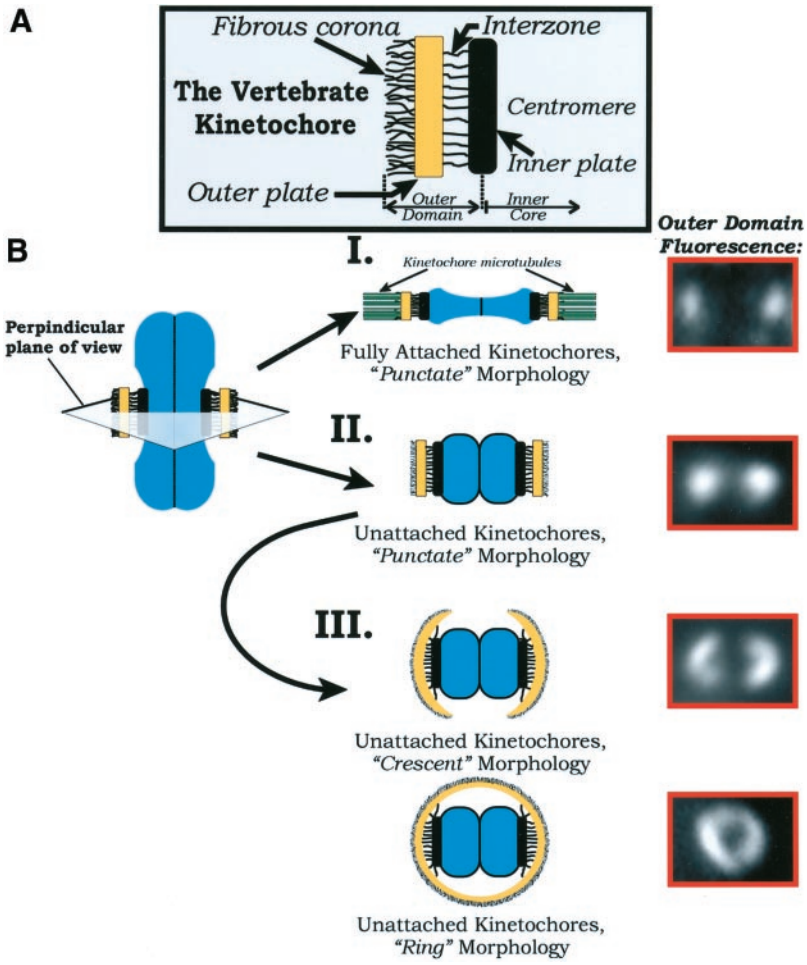

Figure 8. (A) Schematic diagram of the vertebrate kinetochore. Structural domains are labeled according to the model prese nted by Rieder and Salmon (1998). Two major domains are delineated for the purposes of this article: the inner core, consisting of the inner plate proximal centromere region, and the outer domain, which extends from the inner plate through the interzone, outer plate, and fibrous corona. (B) Illustration of the reversible morphological changes in the kinetochore outer domain between metaphase kinetochores with their full complement of kinetochore microtubules (I) and kinetochores depleted of kinetochore microtubules in cells where microtubule polymerization is blocked for prolonged periods of time with 20 μM nocodazole (II and III). We have taken a perpendicular cross section of a chromosome through the centromere region (top, center). Electron microscopy has shown that coronal fibers are difficult to detect at kinetochores of metaphase chromosomes (Rieder, 1982; Cassimeris *et al.*, 1990), and by immunofluorescence the outer domain remains compact, appearing as punctate or oblate points of fluorescence (I). After depletion of kinetochore microtubules in nocodazole, the outer plate region appears extended and the coronal fibers dense in electron micrographs (Rieder, 1982; Cassimeris *et al.*, 1990), whereas our fluorescence analysis shows that the outer domain can expand outward around the centromere forming crescent or ring morphologies (III) in prolonged nocodazole incubations. These morphological changes in the kinetochore outer domain are reversible with microtubule reassembly and kinetochore microtubule formation.

DISCUSSION

Microtubules Regulate the State of Kinetochore Outer Domain Assembly

Our results show three different microtubule-dependent states of mitotic kinetochore outer domain assembly (Figure 8). First, kinetochores in cells depleted of all spindle microtubules by nocodazole treatment exhibit enhanced outer domain protein concentrations and expanded crescent and ring morphologies. Second, prometaphase kinetochores with no or few kinetochore microtubules, but surrounded by nonkinetochore microtubules, exhibit enhanced outer domain protein concentrations, but no crescent or ring morphologies. Third, metaphase kinetochores, with a full complement of kinetochore microtubules as well as surrounding nonkinetochore spindle microtubules, exhibit reduced outer domain protein concentrations, particularly for Mad2 and cytoplasmic dynein, and no crescent or ring morphologies. In contrast, inner core protein assembly appears independent of either nonkinetochore or kinetochore microtubules because we observed little change in the amounts of CREST staining at kinetochores under all the conditions tested. In the future, the independence observed for CREST antigens CENP-A, CENP-B, and CENP-C needs to be tested for other centromere-bound proteins such as the INCENPs, mitotic-centromere–associated kinesin, and Aurora kinase (reviewed in Maney *et al.*, 2000).

Kinetochore Crescent and Ring Morphologies Are Correlated with a Depletion of Kinetochore and Nonkinetochore Microtubules and a Substantial Increase in the Amount of Kinetochore-bound Cytoplasmic Dynein

We found two major differences between unattached prometaphase kinetochores and kinetochores devoid of microtubules in nocodazole-treated cells. We never observed unattached prometaphase kinetochores with extended crescent or ring morphologies that are typical of kinetochores in nocodazole-treated cells. The MG-132 experiments show that prolonged mitosis does not induce expansion of kinetochores on metaphase chromosomes in cells where microtubule disassembly has not occurred. In addition, the concentration, relative to metaphase kinetochores, of cytoplasmic dynein on unattached prometaphase kinetochores (~5-fold) was more than an order of magnitude less than measured for kinetochores in nocodazole-treated cells (at least 50- to 100-fold) (Figures 5 and 7). The amounts of

BubR1, CENP-E, and Mad2 did not change as substantially between unattached kinetochores in prometaphase cells and kinetochores in nocodazole-treated cells (Figures 5 and 7). Thus, the formation of the extended crescent and ring morphologies of the kinetochore outer domain is correlated with absence of microtubules and substantial increases in the amounts of kinetochore cytoplasmic dynein. In this regard, prophase kinetochores lack surrounding microtubules like kinetochores in nocodazole-treated prometaphase cells, but exhibit no crescent or ring morphologies and no bound cytoplasmic dynein (Figure 2).

In nocodazole-treated prometaphase cells, all the outer domain proteins as well as the 3F3/2 antigen uniformly colocalized with cytoplasmic dynein in the crescents and rings (Figure 1). This indicates that accumulation of cytoplasmic dynein and the expansion into crescent and ring morphologies spreads out the binding sites for BubR1, CENP-E, and Mad2. The expanded crescents and rings likely reflect an enhancement of the outer plate coronal filaments because they contain cytoplasmic dynein and CENP-E (reviewed in Rieder and Salmon, 1998; Maney *et al.*, 2000).

A simple hypothesis to explain these microtubule-dependent differences between unattached prometaphase kinetochores and the kinetochores in nocodazole-treated cells is that kinetochore interactions with nonkinetochore microtubules prevents unattached prometaphase kinetochores from forming crescent or ring morphologies or accumulating high concentrations of cytoplasmic dynein at the kinetochore. By this mechanism, kinetochore expansion requires a minimal duration without microtubule interactions and no prometaphase kinetochores lack microtubule interactions for long enough to exceed this duration. This explains why the kinetochore crescent and ring morphologies rapidly disappear upon nocodazole washout and spindle microtubule reassembly (Figure 6).

The microtubule motor activity of cytoplasmic dynein may be a key factor in understanding the dynamics of cytoplasmic dynein assembly at kinetochores. Cytoplasmic dynein translocates toward the minus ends of microtubules that are oriented toward the spindle poles (Inoue and Salmon, 1995). This motor activity would provide a force for driving the dissociation of cytoplasmic dynein in the presence of proximal nonkinetochore microtubules in prometaphase, but not when microtubules are depleted by nocodazole. Depletion of microtubules eliminates this dissociation force allowing the accumulation of cytoplasmic dynein from cytoplasmic pools and the expansion of the outer domain into crescents and rings. The dissociation force returns when microtubules reassemble after nocodazole washout, pulling cytoplasmic dynein from the kinetochores. Cytoplasmic dynein is further depleted by approximately sixfold from prometaphase kinetochores as they acquire their full complement of metaphase kinetochore microtubules (Figure 5). This further depletion may also be explained by the enhancement of cytoplasmic dynein dissociation driven by the additional opportunities for motor activity on the kinetochore microtubules. Dynein-driven transport along microtubules could also contribute to microtubule-dependent depletion of other outer domain proteins and explain the poleward transport of fluorescent Mad2 from unattached kinetochores (Howell *et al.*, 2000).

Although this dynein-driven depletion of outer domain proteins is an attractive hypothesis to explain the difference between the morphology of prometaphase and nocodazole-treated kinetochores, there are other possibilities that need testing in the future. Nonkinetochore microtubules could provide a substrate for depleting cytoplasmic dynein from the cytoplasmic pool, reducing its association with kinetochores and reducing kinetochore expansion. Spindle microtubules might concentrate the activities of kinases or phosphatases and/or their regulators (Gundersen and Cook, 1999) that could regulate the rates of association and dissociation of cytoplasmic dynein and the expansion of the kinetochore outer domain. Finally, expansion may require that neither sister kinetochore be attached to microtubules. This is not likely to be dependent on tension because kinetochores in taxol-treated metaphase cells lack tension but do not exhibit expanded crescents (Figure 6).

Depletion of Outer Domain Proteins during Maturation of Metaphase Kinetochores Is Dominated by Microtubule Attachment and Not Controlled Directly by Changes in Tension

We found no effects on metaphase kinetochore protein composition (Figures 6 and 7 and Table 2) from the enhanced assembly of nonkinetochore microtubules that occurs with taxol stabilization (Waters *et al.*, 1996a). McEwen *et al.* (1997) also found little change in the number of metaphase kinetochore microtubules. Thus, whatever effects nonkinetochore spindle microtubules may have on kinetochore assembly are achieved by the normal degree of spindle microtubule assembly in prometaphase and metaphase. As shown earlier for Mad2 (Waters *et al.*, 1998) and Bub3 (Martinez-Exposito *et al.*, 1999), we found that loss of tension at metaphase kinetochores treated with taxol did not change the integrated fluorescence intensities of CENP-E, BubR1, or cytoplasmic dynein. Thus, for these outer domain proteins in PtK1 cells, microtubule attachment is dominant over contributions from changes in tension in regulating their amounts at metaphase kinetochores. This may be a general property of kinetochores because a recent report by King *et al.* (2000) has shown that the depletion of cytoplasmic dynein and CENP-E at kinetochores of meiotic grasshopper spermatocytes depends on kinetochore microtubule formation, not directly on tension. However, tension appears to indirectly regulate kinetochore assembly by stabilizing kinetochore microtubule attachment (King and Nicklas, 2000).

Differential Changes in Kinetochore Assembly with Kinetochore Microtubule Formation

Compared with unattached prometaphase kinetochores, the outer domains of kinetochores on metaphase chromosomes are depleted significantly of both microtubule motor proteins that play a role in microtubule attachment and the spindle checkpoint proteins that produce the wait-anaphase signal. We found that the depletion of these proteins can be classified into two groups, depending on the magnitude of depletion. Mad2 was in one group by itself, because it is depleted by 100-fold with kinetochore microtubule formation (Figure 5). Our second group includes CENP-E, cytoplasmic dynein, and BubR1, which are depleted three- to sixfold by kinetochore microtubule formation. Quantitative

immunofluorescence measurements have also shown a 3.5-fold decrease for Bub3 in HeLa cells (Martinez-Exposito *et al.*, 1999) between unattached and attached kinetochores on metaphase-aligned chromosomes. Bub3 targets Bub1 and BubR1 to kinetochores (Taylor and McKeon, 1997). Qualitative immunofluorescence assays indicate that Bub1 depletion at metaphase kinetochores in HeLa and U2OS mammalian cells is similar to that of BubR1 (Jablonski *et al.*, 1998). Thus, our measurements for BubR1 predict that Bub1, like Bub3 is depleted by ~3.5-fold as chromosomes achieve their metaphase complement of kinetochore microtubules. Similar to our measurements, a threefold depletion of CENP-E from HeLa kinetochores by kinetochore microtubule formation has been found by immunogold electron microscopy (Yao *et al.*, 1997). Biochemical analysis has shown that CENP-E and BubR1 physically interact, which may explain why they deplete by similar amounts with microtubule attachment (Chan *et al.*, 1999; Yao *et al.*, 2000). In the King *et al.* (2000) study of meiosis I grasshopper spermatocytes, they found 10- and 3-fold lower concentrations of cytoplasmic dynein and CENP-E, respectively, on metaphase kinetochores in comparison to kinetochores on detached chromosomes. These values are very similar to those we measured for mitotic mammalian tissue cells. Visual inspection of immunofluorescently stained kinetochores has shown that Mad1, which targets Mad2 to kinetochores, decreases substantially with kinetochore microtubule formation (Chen *et al.*, 1998; Chan *et al.*, 2000; Campbell *et al.*, 2001), but the reduction has not been quantitated. Mad1 binds tightly to Mad2 (Chen *et al.*, 1999), so like Mad2, it is likely to be substantially depleted by microtubule attachment. In summary, the above-mentioned analysis indicates that Bub1, BubR1, Bub3, CENP-E, and cytoplasmic dynein deplete by three- to fivefold with kinetochore microtubule formation in mammalian cells and all these proteins persist on metaphase kinetochores. Mad2 is distinct from this group because it becomes nearly undetectable on metaphase kinetochores.

The above-mentioned quantitative analysis provides direct support for the idea that unattached prometaphase kinetochores have significantly larger amounts of microtubule motor proteins to enhance the recruitment of kinetochore microtubules, as well as larger amounts of the spindle checkpoint proteins to amplify the inhibitory signal that delays anaphase onset (Rieder and Salmon, 1998; Howell *et al.*, 2000). Depletion of these proteins correlates with the twofold decrease in kinetochore width between prometaphase and metaphase when it becomes fully occupied with kinetochore microtubules (Rieder, 1982) and the decrease in density of the coronal filaments, which extend out of the outer plate (Figure 8; Rieder, 1982; Salmon, 1989; Cassimeris *et al.*, 1990). The substantial increase in the amount of cytoplasmic dynein on kinetochores in nocodazole-treated cells may have a function in enhancing the probability of recruiting microtubules to kinetochores under conditions where microtubule density is very low.

The leading kinetochore on chromosomes congressing to the metaphase plate differs from the trailing kinetochore in two ways. First, leading kinetochores are attached to one to three kinetochore microtubules, whereas trailing kinetochores have 13 or more kinetochore microtubules (Figure 2A; McEwen *et al.*, 1997). Second, leading kinetochores have the higher concentrations of cytoplasmic dynein and CENP-E typical of unattached kinetochores, whereas the trailing kinetochore is often depleted to the lower metaphase levels because of their attached kinetochore microtubules. Although the leading kinetochore may have fewer kinetochore microtubules, the higher concentrations of motor proteins may make it the dominant pulling force on the centromere, biasing the trailing kinetochore into a nonpulling state as described by Skibbens *et al.* (1993), and Rieder and Salmon (1994, 1998). This bias could generate persistent chromosome movement to the metaphase plate (Waters *et al.*, 1996b) where both the leading and trailing sister kinetochores are able to acquire a full complement of kinetochore microtubules and become depleted equally in their concentrations of CENP-E and cytoplasmic dynein (Rieder and Salmon, 1998).

Mad2, unlike Bub1, BubR1, and Bub3, is depleted, by two orders of magnitude on metaphase kinetochores. This extensive depletion of Mad2 is predicted by Mad2 being part of the inhibitory signal sent from kinetochores lacking the correct complement of kinetochore microtubules. The current model is that unattached kinetochores inhibit anaphase onset (Rieder *et al.*, 1995) by catalyzing Mad2 binding and inhibition of cdc20 protein, producing in the cytoplasm inhibited anaphase-promoting complex (Chen *et al.*; 1998; Gorbsky *et al.*, 1998; Hardwick *et al.*, 2000; Howell *et al.*, 2000). The near absence of Mad2 on metaphase kinetochores indicates that kinetochore production of the Mad2 inhibitory activity is turned off.

Future Considerations

The molecule mechanisms that regulate the assembly/disassembly and activity of Mad2 and the more resident mitotic spindle checkpoint proteins such as Bub1, BubR1, and Bub3 remain an important unanswered question. Neither CENP-E nor cytoplasmic dynein appear required for Mad2 or BubR1 binding to kinetochores in tissue cells. Depletion of kinetochore CENP-E (Schaar *et al.*, 1997; Chan *et al.*, 1999; Yao *et al.*, 2000) suppresses kinetochore microtubule formation, but unattached kinetochores have high amounts of both Mad2 and BubR1 and the spindle checkpoint is activated. Cytoplasmic dynein at kinetochores also does not appear essential for Mad2 binding to unattached kinetochores because we found Mad2 highly concentrated on kinetochores in prophase nuclei that show no staining for cytoplasmic dynein. In addition, depletion of zw10, rod, or dynein/dynactin also does not prevent Mad1, Mad2, or BubR1 from binding unattached prometaphase kinetochores (Chan *et al.*, 2000), but zw10 and rod, proteins that target cytoplasmic dynein to kinetochores, do appear required for maintenance of checkpoint activity (Chan *et al.*, 2000; Basto *et al.*, 2000). Howell *et al.* (2000) has shown that Mad2 binding sites are transported poleward from unattached kinetochores to the poles. Because this is the direction cytoplasmic dynein translocation along microtubules, cytoplasmic dynein motor activity may be important not only for reducing the size of the kinetochore, as discussed above, but also for turning off spindle checkpoint activity at kinetochores.

ACKNOWLEDGMENTS

We thank Gordon Chan and Sandra Jablonski for providing the 1.6 CENP-E and hBubR1 affinity-purified antibodies and the members

of the Bloom and Salmon labs for help and comments on the manuscript. This study was supported by National Institutes of Health Grant GM-24364 to E.D.S. and National Institutes of Health Grants GM-44762 and CA-06927, the March of Dimes Foundation, and an appropriation from the Commonwealth of Pennsylvania to T.Y.

REFERENCES

Amon, A. (1999). The spindle checkpoint. Curr. Opin. Genet. Dev. *9*, 69–75.

Basto, R., Gomes, R., and Karess, R.E. (2000). Rough Deal and Zw10 are required for the metaphase checkpoint in *Drosophila*. Nat. Cell Biol. *2*, 939–943.

Campbell, M.S., Chan, G.K.T., and Yen, T.J. (2001). Mitotic checkpoint proteins HsMAD1 and HsMAD2 are associated with nuclear pore complexes in interphase. J. Cell Sci. *114*, 953–963.

Campbell, M.S., and Gorbsky, G.J. (1995). Microinjection of mitotic cells with the 3F3/2 anti-phosphoepitope antibody delays the onset of anaphase. J. Cell Biol. *129*, 1195–1204.

Cassimeris, L., Rieder, C.L., Rupp, G., and Salmon, E.D. (1990). Stability of microtubule attachment to metaphase kinetochores in PtK1 cells. J. Cell Sci. *96*, 9–15.

Chan, G.K.T., Jablonski, S.A., Starr, D.A., Goldberg, M.L., and Yen, T.J. (2000). Human Zw10 and ROD are mitotic checkpoint proteins that bind to kinetochores. Nat. Cell Biol. *2*, 944–947.

Chan, G.K.T., Jablonski, S.A., Sudakin, V., Hittle, J.C., and Yen, T.J. (1999). Human BUBR1 is a mitotic checkpoint kinase that monitors CENP-E functions at kinetochores and binds the cyclosome/APC. J. Cell Biol. *146*, 941–954.

Chan, G.K.T., Schaar, B.T., and Yen, T.J. (1998). Characterization of the kinetochore binding domain of CENP-E reveals interactions with the kinetochore proteins CENP-F and hBUBR1. J. Cell Biol. *143*, 49–63.

Chen, R.-H., Brady, D.M., Smith, D., Murray, A.W., and Hardwick, K.G. (1999). The spindle checkpoint of budding yeast depends on a tight complex between the Mad1 and. Mad2 proteins. Mol. Biol. Cell. *10*, 2607–2618.

Chen, R.-H., Shevchenko, A., Mann, M., and Murray, A.W. (1998). Spindle checkpoint protein Xmad1 recruits Xmad2 to unattached kinetochores. J. Cell Biol. *142*, 283–295.

Chen, R.-H., Waters, J.C., Salmon, E.D., and Murray, A.W. (1996). Association of spindle assembly checkpoint component Xmad2 with unattached kinetochores. *Science 274*, 242–246.

Cimini, D., Howell, B.J., Maddox, P.S., Khodjakov, A., Degrassi, F., and Salmon, E.D. (2001). Merotelic kinetochore orientation is a major mechanism of aneuploidy in mitotic mammalian tissue cells. J. Cell Biol. *153*, 517–527.

Clute, P., and Pines, J. (1999)., Temporal and spatial control of cyclin B destruction in metaphase. Nat. Cell Biol. *1,* 82–87.

DeBrabender, M., Guens, G., Nuydens, R., Willebrords, R., and DeMey, J. (1981). Microtubule assembly in living cells after release from nocodazole block: the effects of metabolic inhibitors, taxol, and pH. Cell Biol. Int. Rep. *5*, 913–920.

Dujardin, D., Wacker, U.I., Moreau, A., Schroer, T.A., Rickard, J.E., and De Mey, J.R. (1998). Evidence for a role of CLIP-170 in the establishment of metaphase chromosome alignment. J. Cell Biol. *141*, 849–862.

Earnshaw, W.C., Ratrie, H. III, and Stetten, G. (1989). Visualization of centromere proteins CENP-B and CENP-C on a stable dicentric chromosome in cytological spreads. Chromosoma *98*, 1–12.

Earnshaw, W.C., and Rothfield, N. (1985). Identification of a family of human centromere proteins using autoimmune sera from patients with scleroderma. Chromosoma *91*, 313–321.

Echeverri, C.J., Paschal, B.M., Vaughan, K.T., and Vallee, R.B. (1996). Molecular characterization of the 50-kD subunit of dynactin reveals function for the complex in chromosome alignment and spindle organization during mitosis. J. Cell Biol. *132*, 617–633.

Gorbsky, G.J., Chen, R.-H., and Murray, A.W. (1998). Microinjection of antibody to Mad2 protein into mammalian cells in mitosis induces premature anaphase. J. Cell Biol. *141*, 1193–1205.

Gorbsky, G.J., and Ricketts, W.A. (1993). Differential expression of a phosphoepitope at the kinetochores of moving chromosomes. J. Cell Biol. *122*, 1311–1321.

Gundersen, G.G., and Cook, T.A. (1999). Microtubules and signal transduction. Curr. Opin. Cell Biol. *11*, 81–94.

Hardwick, K.G., Johnston, R.C., Smith, D.L., and Murray, A.W. (2000). MAD3 encodes a novel component of the spindle checkpoint which interacts with Bub3p, Cdc20p, and Mad2p. J. Cell Biol. *148*, 871–882.

Howell, B.J., Hoffman, D.B., Fang, G., Murray, A.W., and Salmon, E.D. (2000). Visualization of Mad2 dynamics at kinetochores, along spindle fibers, and at spindle poles in living cells. J. Cell Biol. *150,* 1233–1250.

Inoue, S., and Salmon, E.D. (1995). Force generation by microtubule assembly/disassembly in mitosis and related movements. Mol. Biol. Cell *6*, 1619–1640.

Jablonski, S.A., Chan, G.K.T., Cooke, C.A., Earnshaw, W.C., and Yen, T.J. (1998). The hBUB1 and hBUBR1 kinases sequentially assemble onto kinetochores during prophase with hBUBR1 concentrating at the kinetochore plates in mitosis. Chromosoma *107*, 386–396.

Josefsberg, L.B., Galiani, D., Dantes, A., Amsterdam, A., and Dekel, N. (2000). The proteasome is involved in the first metaphase-anaphase transition in meiosis in rat oocytes. Biol. Reprod. *62*, 1270–1277.

Khodjakov, A., and Rieder, C.L. (1996). Kinetochores moving away from their associated pole do not exert a significant pushing force on the chromosome. J. Cell Biol. *135*, 315–327.

King, J.M., Hays, T.S., and Nicklas, R.B. (2000). Dynein is a transient kinetochore component whose binding is regulated by microtubule attachment, not tension. J. Cell Biol. *151*, 739–748.

King, J.M., and Nicklas, R.B. (2000). Tension on chromosomes increases the number of kinetochore microtubules but only within limits. J. Cell Sci. *113*, 3815–3823.

Li, Y., and Benezra, R. (1996). Identification of a human mitotic checkpoint gene: hsMAD2. Science *274*, 246–248.

Luo, X., Fang, G., Coldiron, M., Lin, Y., Kirschner, M.W., and Wagner, G. (2000). Structure of the Mad2 spindle assembly checkpoint protein and its interaction with Cdc20. Nat. Struct. Biol *7*, 224–229.

Maney, T., Ginkel, L.M., Hunter, A.W., and Wordeman, L. (2000). The kinetochore of higher eukaryotes: a molecular view. Int. Rev. Cytol. *194*, 67–131.

Martinez-Exposito, M.J., Kaplan, K.B., Copeland, J., and Sorger, P.K. (1999). Retention of the Bub3 checkpoint protein on lagging chromosomes. Proc. Natl. Acad. Sci. USA *96*, 8493–8498.

McEwen, B.F., Heagle, A.B., Cassels, G.O., Buttle, K.F., and Rieder, C.L. (1997). Kinetochore fiber maturation in PtK1 cells and its implications for the mechanisms of chromosome congression and anaphase onset. J. Cell Biol. *137*, 1567–1580.

Nicklas, R.B. (1997). How cells get the right chromosomes. Science *275*, 632–637.

Nicklas, R.B., Ward, S.C., and Gorbsky, G.J. (1995). Kinetochore chemistry is sensitive to tension and may link mitotic forces to a cell cycle checkpoint. J. Cell Biol. *130*, 929–939.

Rieder, C.L. (1982). The formation, structure and composition of the mammalian kinetochore and kinetochore fiber. Int. Rev. Cytol. *79*, 1–58.

Rieder, C.L., Cole, R.W., Khodjakov, A., and Sluder, G. (1995). The checkpoint delaying anaphase in response to chromosome monorientation is mediated by an inhibitory signal produced by unattached kinetochores. J. Cell Biol. *130*, 941–948.

Rieder, C.L., and Salmon, E.D. (1994). Motile kinetochores and polar ejection forces dictate chromosome position on the vertebrate mitotic spindle. J. Cell Biol. *124*, 223–233.

Rieder, C.L., and Salmon, E.D. (1998). The vertebrate cell kinetochore and its roles during mitosis. Trends Cell Biol. *8*, 310–318.

Salmon, E.D. (1989). Microtubule dynamics and chromosome movement. In: Mitosis, ed. B.R. Brinkley and J. Hyams, New York, NY; Academic Press, 119–181.

Salmon, E.D., Inoue, T., Desai, A., and Murray, A.W. (1994). High resolution multimode digital imaging system for mitosis studies in vivo and in vitro. Biol. Bull. *187*, 231–232.

Schaar, B.T., Chan, G.K.T., Maddox, P., Salmon, E.D., and Yen, T.J. (1997). CENP-E function at kinetochores is essential for chromosome alignment. J. Cell Biol. *139*, 1373–1382.

Shah, J.V., and Cleveland, D.W. (2000). Waiting for anaphase: Mad2 and the spindle assembly checkpoint. Cell. *103*, 997–1000.

Skibbens, R.V., and Hieter, P. (1998). Kinetochores and the checkpoint mechanism that monitors for defects in the chromosome segregation machinery. Annu. Rev. Genet. *32*, 307–337.

Skibbens, R.V., Skeen, V.P., and Salmon, E.D. (1993). Directional instability of kinetochore motility during chromosome congression and segregation in mitotic newt lung cells: a push-pull mechanism. J. Cell Biol. *122*, 59–75.

Taylor, S.S., and McKeon, F. (1997). Kinetochore localization of murine Bub1 is required for normal mitotic timing and checkpoint response to unattached kinetochores. Cell *89*, 727–735.

Thrower, D.A., Jordan, M.A., and Wilson, L. (1996). Modulation of CENP-E organization at kinetochores by spindle microtubule attachment. Cell Motil. Cytoskeleton *35*, 121–133.

Waters, J.C., Chen, R.-H., Murray, A.W., Gorbsky, G.J., Salmon, E.D., and Nicklas, R.B. (1999). Mad2 binding by phosphorylated kinetochores links error detection and checkpoint action in mitosis. Curr. Biol. *9*, 649–652.

Waters, J.C., Chen, R.-H., Murray, A.W., and Salmon, E.D. (1998). Localization of Mad2 to kinetochores depends on microtubule attachment, not tension. J. Cell Biol. *141*, 1181–1191.

Waters, J.C., Mitchison, T.J., Rieder, C.L., and Salmon, E.D. (1996a). The kinetochore microtubule minus end disassembly associated with poleward flux produces a force that can do work. Mol. Biol. Cell *7*, 1547–1558.

Waters, J.C., Skibbens, R.V., and Salmon, E.D. (1996b). Oscillating mitotic newt lung cell kinetochores are, on average, under tension and rarely push. J. Cell Sci. *109*, 2823–2831.

Yao, X., Abrieu, A., Zheng, Y., Sullivan, K.F., and Cleveland, D.W. (2000). CENP-E forms a link between attachment of spindle microtubules to kinetochores and the mitotic checkpoint. Nat. Cell Biol. *2*, 484–491.

Yao, X., Anderson, K.L., and Cleveland, D.W. (1997). The microtubule-dependent motor centromere-associated protein E (CENP-E) is an integral component of kinetochore corona fibers that link centromeres to spindle microtubules. J. Cell Biol. *139*, 435–447.